

## Moderated Poster Presentation I

Friday, January 21, 2005

### 301. Cardiac MRI Within One Week of Coronary Stent Implantation is Safe

Charles X. Kim, MD,<sup>1</sup> Edwin Wu, MD,<sup>2</sup> Daniel C. Lee, MD,<sup>2</sup> Charles J. Davidson, MD,<sup>2</sup> Robert O. Bonow, MD,<sup>2</sup> Mark J. Ricciardi, MD.<sup>2</sup> <sup>1</sup>Feinberg School of Medicine, Northwestern University, Chicago, IL, USA, <sup>2</sup>Feinberg Cardiovascular Institute, Northwestern University, Chicago, IL, USA.

**Introduction:** The clinical utility of cardiac magnetic resonance imaging (cMRI) soon after coronary stent implantation is expanding. The safety of cMRI immediately post stent has not been studied in a large population and ‘information for use’ (IFU) guidelines recommend against MRI for 8 weeks.

**Purpose:** We sought to determine whether cMRI early after coronary stent implantation is safe.

**Methods:** Ninety-four consecutive patients undergoing 96 coronary stent procedures and subsequent cMRI within 7 days were evaluated for sub-acute stent thrombosis, myocardial infarction (MI), death, and restenosis during index hospitalization, at 30 days and 6 months. Both TrueFISP cine and contrast-enhanced MRI were performed using a 1.5 Tesla clinical scanner with advanced, fast gradient systems (Siemens Sonata).

**Results:** The majority (83%) had cMRI within 3 days post-stent (median 2 days). Mean age  $57 \pm 11$  years, 18(19%) female, 22 (23%) diabetic, and mean ejection fraction  $46 \pm 13\%$ . Stent indication was ST elevation MI in 65 (68%), acute coronary syndrome in 21 (22%), and stable angina in 9 (9%). Seventy (73%) received platelet GPIIb/IIIa inhibitor. There was 100% survival follow-up confirmed by Social Security Death Index. Other event follow-up was available in 100%, 94%, and 90% at hospitalization, 30 days, and 6 months, respectively.

	CARDIAC EVENTS		
	In-hospital	30 Day	6 Month
Death	0	0	0
Stent thrombosis	1 (1.0%)	0	0
Restenosis	0	0	2 (2.5%)

The one patient with stent thrombosis had heparin-induced thrombocytopenia. Two MIs were noted at follow-up; neither in the stent artery territory.

**Conclusions:** In this first large study of cardiac MRI within 7 days of coronary stent implantation, in-hospital, 30 day and 6 month cardiac event rates were exceedingly low. These data suggest that cardiac MRI does not confer additional morbidity or mortality and can be performed safely early after coronary stent implantation.

### 302. Safety and Feasibility of High-Dose-Dobutamine Stress MRI for Detection of Myocardial Ischemia: Experience in 400 Consecutive In- and Outpatients.

Rainer Ott, MD,<sup>1</sup> Brigitte Bathgate, MD,<sup>1</sup> Corina Cozub-Poetica, MD,<sup>1</sup> Ralf Banach,<sup>1</sup> Heinz Klues, MD,<sup>2</sup> Volkhard Fiedler, MD.<sup>3</sup> <sup>1</sup>Institute for Cardiovascular MR, Krefeld, Germany, <sup>2</sup>Department of Cardiology, Klinikum Krefeld, Krefeld, Germany, <sup>3</sup>Department of Radiology, Klinikum Krefeld, Krefeld, Germany.

**Introduction:** High-dose dobutamine stress MRI (DSMR) is an accurate modality for diagnosis of myocardial ischemia.

**Purpose:** To evaluate the safety, feasibility and side effects of DSMR in a large unselected in- and outpatient population.

**Methods:** Within 10 months (August 2003 to May 2004) we performed 413 consecutive DSMR studies in 400 in- and outpatients. We used a standardized high-dose dobutamine-atropine protocol at doses of 20,30 and 40 ug/kg/min plus the administration of atropine if needed, until  $\geq 85\%$  of age-predicted heart rate was reached. 3 short-axis and 3 long axis (4,3,2 CV) were acquired at rest and on each level of stresstest (SSFP-cine, Siemens Sonata).

The examination was stopped when target heart rate was reached, on protocol termination or patient request, with new or worsening wall motion abnormalities, severe patient discomfort, severe decrease or increase of blood pressure or severe rhythm disturbances occurred.

**Results:** 278 patients were male, 122 female with a mean age of 63 yrs. 220 patients were outpatients, 180 inpatients. 43.2% (n = 190) of patients had known, 56.8% (n = 210) suspected CAD. In 6 cases (1.5%) could not be performed due to claustrophobia (n = 4; 0.1%) or an unknown LV thrombus (n = 1, 0.02%). In all other cases (n = 407) DSMR was performed successfully.

In the absence of ischemia, target heart was not reached in 28 cases (6.9%), due to non ceased betablocker medication in 3 cases (0.7%) or to limiting side effects in 25 cases (6.2%): Severe increase (n = 6; 1.5%) or decrease (n = 3; 0.8%) of blood pressure, severe headache (n = 1; 0.2%), nausea (n = 2; 0.4%), claustrophobia (n = 4, 1%), dyspnoea (n = 2, 0.4%), fast paroxysmal atrial fibrillation (n = 3; 0.8%), sustained (n = 2; 0.4%) and non-sustained tachycardia (n = 2, 0.4%).

Minor side effects not leading to test termination occurred in 88 cases (21,6%) including chest pain (n = 44; 10.8%), ventricular and supraventricular extrasystoly (n = 38; 9.3%), paroxysmal atrial fibrillation (n = 5; 1,2%) and headache (n = 1; 0.2%).

Sixty patients (15%) had a positive stresstest, whereas in 340 patients (85%) no new or worsening wall motion abnormalities were detected.

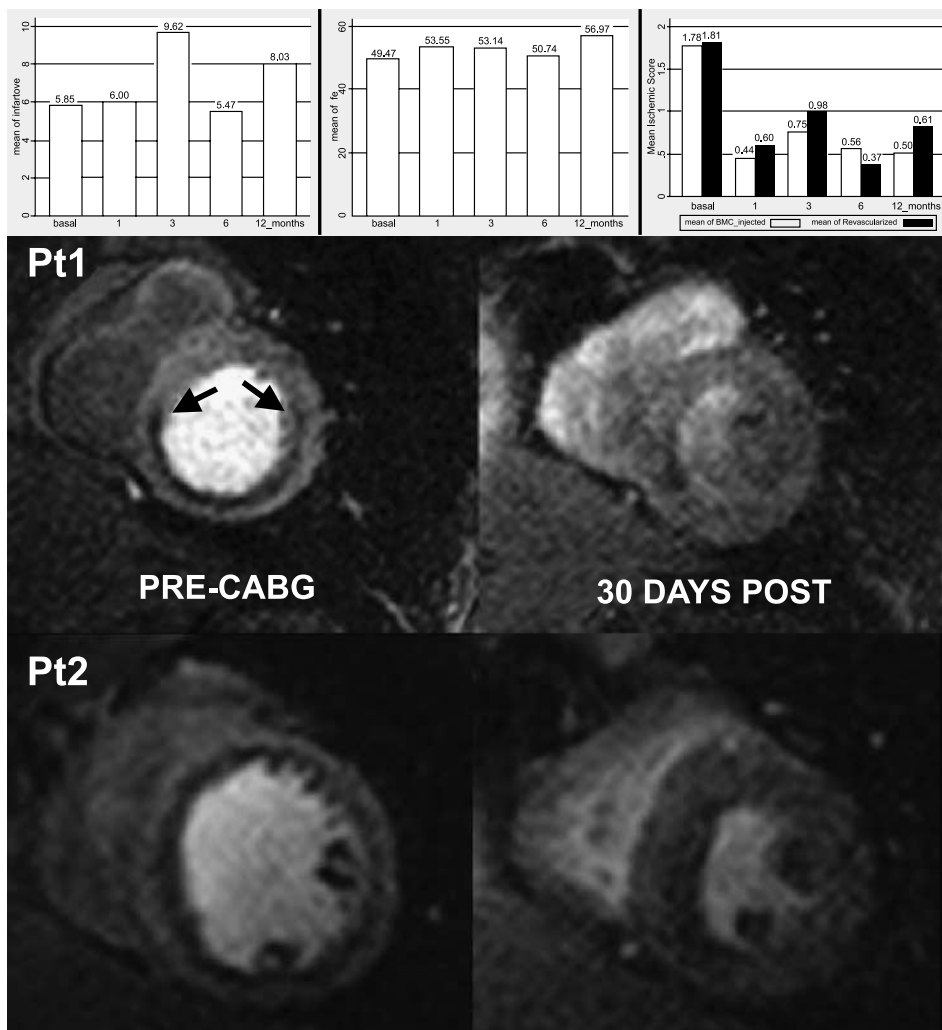
**Conclusions:** DSMR is a safe, feasible and robust method for detecting myocardial ischemia in in- and outpatients. But precautions for patients safety are a must.

### 303. Myocardial Perfusion Improvement Detected by MRI in Patients Undergoing Surgical Revascularization and Bone Marrow Cells Injection—One Year Follow-Up

Carlos E. Rochitte, Victor M. A. MonsÃ£o, MD, Luis H. Gowdak, MD, JosÃ E. Krieger, MD, Marcello Zapparolli, MD, JosÃ R. Parga, MD, Luiz Francisco Ãvila, MD, JosÃ Antonio Franchini Ramires, MD, SÃrgio A. Oliveira, MD. *Cardiology, Heart Institute-InCor- University of SÃo Paulo Medical School, Sao Paulo, Brazil.*

**Introduction:** Adult bone marrow cells (BMC) are involved in tissue repair and vascular growth, and might be used therapeutically in ischemic tissues. There is growing evidence that adult bone marrow cells (BMC) have the potential to contribute to angiogenesis, myogenesis and matrix remodeling which might be explored therapeutically in ischemic heart disease.

**Objectives:** To assess myocardial ischemia by MRI stress myocardial perfusion during the first year (four time points)



after intramyocardial injection of autologous BMC in patients (pt) undergoing incomplete surgical revascularization for diffuse coronary artery disease (CAD). We also evaluated one-year safety and tolerability, as well as, left ventricular function and myocardial delayed enhancement by MRI.

**Methods:** 10 pt (8 men), age = 59.1 years-old, with 3-vessel disease, limiting angina (class III–IV CCS), and who were not optimal candidates for “complete” surgical revascularization due to the extension of the disease were enrolled. BMC were obtained immediately prior to surgery, and the lymphomonocytic fraction separated by density gradient centrifugation. During surgery, injections of BMC were performed in the non-grafted areas of ischemic myocardium. Pt underwent MRI study in a 1.5T CV/i GE scanner to evaluate: myocardial perfusion during stress with dipyridamole (0.56mg/kg/4min), using a hybrid gradient-echo with multiple read-out; left ventricular function (left ventricular ejection fraction, end diastolic, end systolic volumes and mass) by cine MRI using a steady-state gradient-echo (FIESTA); and myocardial fibrosis quantification by myocardial delayed enhancement technique (inversion recovery prepared gradient-echo). MR studies were performed before, 30 days, 3 months, 6 months and one year after surgery. Myocardial perfusion was analyzed by 2 observers and classified using a 17-segment model and a perfusion defect score (0 for no perfusion defect, 1 for mild defect and 2 for moderate/severe defect). Mean scores of the ischemic segments on the baseline study were analyzed and comparison performed between revascularized segments versus BMC injected segments.

**Results:** BMC injected segments included the inferior wall in 7 pts and the anterior wall in 3. There were no major complications (including malignant arrhythmias) or deaths. All patients remained free of angina in the follow-up. There were no differences in infarct size, LV ejection fraction over the 4 time-points in the first year of follow-up (Graph). Myocardial perfusion improved in both BMC injected and revascularized segments (Graph) by a significant reduction of the mean ischemic score in all time-points compared to baseline score ( $1.8 \pm 0.4$  vs.  $0.4 \pm 0.7$ ,  $0.8 \pm 0.8$ ,  $0.6 \pm 0.6$ ,  $0.5 \pm 0.4$ ,  $p = 0.004$  and  $1.8 \pm 0.3$  vs.  $0.6 \pm 0.5$ ,  $1.0 \pm 0.7$ ,  $0.4 \pm 0.6$ ,  $0.8 \pm 0.8$ ,  $p = 0.015$ ). The figure depicts 2 patients with clear reduction of perfusion defect from baseline to first month.

**Conclusions:** MRI was able to detect precisely myocardial perfusion improvement after BMC implant associated to CABG. This improvement occurred mainly in the first month after procedure. The precise and accurate myocardial perfusion improvement detection by MRI indicates that this technique may be the best choice to evaluate patients submitted to stem-cell therapies. In the long-term, one-year follow-up, intramyocardial injection of autologous BMC is safe, well-tolerated and did not generate new areas of myocardial fibrosis over one-year follow-up. Moreover, BMC may have contributed to decrease myocardial ischemia in non-grafted areas. This strategy could lead to a new therapeutic option for the treatment of patients suffering from a

more advanced (diffuse) CAD not suitable for complete myocardial revascularization.

### **304. Time from Symptom Onset to Reperfusion and Influence on Infarct Size in Patients with ST-Elevation Myocardial Infarction Reperfused By Prehospital Fibrinolysis or Prehospital Initiated Facilitated Percutaneous Intervention**

Holger Thiele, Mathias J. Kappl, Josef Niebauer, Enno Boudriot, Gerhard Schuler. *Cardiology, University of Leipzig-Heart Center, Leipzig, Germany.*

**Introduction:** The time from symptom onset to reperfusion has strong effects on the final infarct size and subsequently on mortality for STEMI patients treated by fibrinolysis. In patients reperfused by percutaneous coronary intervention (PCI) the final infarct size has been shown to be independent from the time from symptom onset to reperfusion and the effects on mortality are attenuated.<sup>1</sup> The time from symptom onset to reperfusion and the influence on the final infarct size has not been studied for patients treated very early by either prehospital fibrinolysis or prehospital initiated facilitated PCI.

**Purpose:** We hypothesized that the time from symptom onset to reperfusion would affect the final infarct size assessed by magnetic resonance imaging (MRI).

**Methods:** In the Leipzig prehospital fibrinolysis study patients with a STEMI were randomized to either a prehospital fibrinolytic therapy ( $n = 82$ ) or a prehospital initiated facilitated PCI after prehospital fibrinolysis ( $n = 82$ ). The time from symptom onset to reperfusion and the ST-segment resolution at 90 min were assessed for all patients. Patients were divided into the following 3 groups defined by tertiles of the time-to-treatment interval: lower tertile ( $<120$  min), middle tertile (120–240 min), and upper tertile ( $>240$ –360 min). ST-segment resolution was defined as complete ( $\geq 70\%$ ), incomplete ( $<70\%$  to 30%), or no resolution ( $<30\%$ ).

At 6 months follow-up in 134 patients cine loops of the complete heart in short and horizontal long-axis planes were acquired using a steady-state free precession technique (TR/TE/flip = 3.2/1.2/60). Additionally, delayed enhancement images covering the whole ventricle were acquired 10–20 min after a double-bolus of Gadolinium-BOPTA (Gadovist, Schering, Germany) using a 3 D inversion recovery gradient echo sequence (TR/TE/flip 2.8/1.1/15) with the inversion time adapted to null normal myocardium. Infarct size was determined as the percentage of the left ventricular mass.

**Results:** The time interval from symptom onset to reperfusion had a significant influence on final infarct size for the overall patient population. In the lower tertile the final infarct size was  $7.7 \pm 8.1\%$  versus  $12.1 \pm 10.6\%$  in the middle tertile ( $p = 0.04$  versus lower tertile) and  $12.7 \pm 6.9\%$  in the upper tertile ( $p = 0.03$  versus lower tertile). In the

group of patients treated by prehospital fibrinolysis the final infarct size was  $10.2 \pm 9.8\%$  in the lower,  $15.6 \pm 12.6\%$  in the middle, and  $12.8 \pm 8.5\%$  in the upper tertile ( $p = 0.03$ ). In patients treated by prehospital initiated PCI the final infarct size was  $5.2 \pm 4.9\%$  in the lower,  $9.1 \pm 6.0\%$  in the middle and  $13.3 \pm 7.0\%$  in the upper tertile ( $p = 0.01$ ). In patients treated by prehospital fibrinolysis alone the final infarct size was greater in the lower ( $p = 0.006$ ) and middle tertile ( $p = 0.03$ ) in comparison to facilitated PCI.

The ST-segment resolution also correlated significantly with the final infarct size ( $r = -0.35$ ,  $p = 0.005$ ). In the groups with complete, partial, and no resolution the final infarct size was  $14.5 \pm 9.3\%$ ,  $14.2 \pm 8.8\%$ , and  $6.7 \pm 7.8\%$  ( $p < 0.001$ ), respectively.

**Conclusions:** The time from symptom onset to reperfusion influences the final infarct size for either prehospital fibrinolysis or facilitated PCI. A prehospital initiated facilitated PCI approach is superior to prehospital fibrinolysis alone. This underlines the assumed pathophysiological link between early restoration of the flow and perfusion in the infarct related artery, which is known as the “wavefront phenomenon.”

### 305. Discrimination of Ischemic vs. Non-ischemic Cardiomyopathy Among Patients with Heart Failure Using Combined Coronary MRI and Delayed Enhancement MR

Thomas H. Hauser, Susan B. Yeon, Evan Appelbaum, Kraig V. Kissinger, Lois Goepfert, Neil M. Rofsky, Warren J. Manning. *Cardiovascular Division, Beth Israel Deaconess Medical Center, Boston, MA, USA.*

**Introduction:** Heart failure (HF) is increasingly prevalent in the United States. Coronary artery disease (CAD) is the most common cause of HF and the combination of HF and CAD is frequently treated with mechanical revascularization and device implantation. Definitive determination of an ischemic vs. non-ischemic etiology of HF usually requires invasive x-ray coronary angiography. Both coronary magnetic resonance imaging (cMRI) and delayed enhancement magnetic resonance (DE-MR) have shown promise in the non-invasive identification of CAD in patients with HF. We hypothesized that the combination of cMRI and DE-MR would have superior performance to either test alone.

**Methods:** A consecutive series of patients with left ventricular ejection fraction  $< 40\%$  by echocardiography were evaluated with cMRI and DE-MR. cMRI was performed using a submillimeter resolution free-breathing navigator gated/corrected T2 prep targeted 3D turbo field echo sequence after the administration of 2.5 mg sublingual isosorbide dinitrate. DE-MR images were obtained 15 minutes after injection of a total of 0.2 mmol/kg gadolinium contrast. Evidence of multi-vessel CAD on cMRI or any evidence of DE was considered evidence of CAD. For the combined

assessment, evidence of CAD by either test was considered a positive MR result.

**Results:** The study cohort consisted of 11 men and 10 women. The mean age was  $51 \pm 12$ . The mean ejection fraction was  $27 \pm 9$ . CAD risk factors included diabetes ( $n = 6$  [29%]), hypertension ( $n = 11$  [52%]), and dyslipidemia ( $n = 8$  [38%]). CAD proven by x-ray angiography or documented myocardial infarction was present in 8 (38%). The cause of HF in the remaining subjects was idiopathic in 12 (57%) and cardiotoxic chemotherapy in 1 (5%). cMRI yielded interpretable images in 17 (81%) subjects. DE-MR yielded interpretable images in all (100%) subjects. The test characteristics for the combined assessment and for cMRI or DE-MR alone are shown in the Table.

**Conclusions:** Combined assessment with cMRI and DE-MR was more accurate than DE-MR alone. cMRI alone was superior to DE-MR and the combined assessment, but interpretable data were not obtained in all subjects.

Test Characteristics for the Detection of CAD Using cMRI and DE-MR

	cMRI N = 17	DE-MR N = 21	Combined Assessment N = 21
Sensitivity	100%	75%	100%
Specificity	100%	92%	92%
Positive predictive value	100%	86%	89%
Negative predictive value	100%	86%	100%

### 306. MR-based Cardiac Electromechanical Mapping in Ischemic Heart

Hiroshi Ashikaga, MD, Steven R. Mickelsen, BA, Daniel B. Ennis, PhD, Peter Kellman, PhD, Han Wen, PhD, Elliot R. McVeigh, PhD. *National Heart, Lung and Blood Institute, National Institutes of Health, Bethesda, MD, USA.*

**Introduction:** Sudden cardiac death accounts for approximately 50% of cardiovascular mortality, resulting in more than 400,000 deaths annually in the US. Most cases are associated with prior myocardial infarction (MI), and the majority of sudden cardiac death results from reentry ventricular tachycardia. MI confers significant heterogeneity in material property of the myocardium, and regions of greater compliance that experience greater relative stretch during dynamic ventricular loading may provide foci of stretch-activated arrhythmias that serve as a trigger to initiate fatal ventricular tachyarrhythmia.

**Purpose:** We developed a cardiac electromechanical mapping technique using high-resolution DENSE and a 247-lead epicardial electrical sock, and qualitatively assessed anatomical correlation of abnormal electromechanics

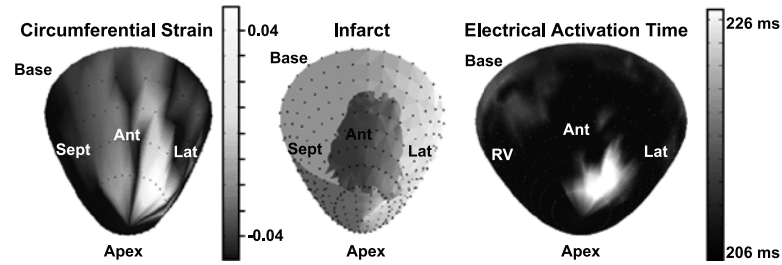


**Figure 1.** Viewing LV anterior wall from the apex.

with reference to the MI boundary in chronic post-MI hearts in vivo.

**Methods:** Six dogs underwent MR studies 3 weeks after creating anterior MI by occluding proximal LAD for 2 hours with a balloon angioplasty catheter. All MR studies were conducted in Siemens Sonata 1.5T scanner. MI location and geometry were evaluated with a high-resolution delayed hyperenhancement inversion recovery sequence following intravenous injection of a contrast agent (Gd-DTPA, Berlex Magnevist) at 0.2 mmol/kg (BW ± 140Hz/Px, TE/TR 4.7/32 ms, 30° readout flip angle, FOV 119 × 200 mm<sup>2</sup>, 122 × 256 image matrix, slice 3.0 mm). Epicardial circumferential strain was calculated from 3D displacement fields in five short axis slices using a high-resolution DENSE sequence (FOV 175 × 350 mm<sup>2</sup>, 96 × 250 image matrix, slice 8.0 mm). Isochrone map of the epicardial electrical activation time was determined using 247-lead sock electrodes.

**Results:** Circumferential strain map (Figure 1) showed abnormal myocardial stretch in the anterior MI regions and akinetic areas in the septal and lateral wall. The region of abnormal strain extended far beyond the MI boundary. In contrast, the region of delayed electrical activation, defined as the region with a greater than 50% delay, was over the MI region, but was smaller than the MI boundary, likely due to a complex transmural 3-D geometry of the infarct structure.

**Conclusions:** The abnormal mechanics region is larger than the MI region, whereas delayed electrical activation region is smaller than the MI region. The resultant large area with abnormal mechanics and normal electrical activation in the MI border zone may provide a potential electro-anatomical substrate for ventricular tachyarrhythmia via stretch activated ectopy.

### 307. Determination of Association Between Carotid Atherosclerosis and High Density Lipoprotein Subfractions by High Resolution MRI

Milind Y. Desai, Annabelle Rodriguez, MD, Gary Gerstenblith, MD, Sachin Agarwal, MD, MPH, David A. Bluemke, MD, PhD, Joao A. C. Lima, MD. *Johns Hopkins University, Baltimore, MD, USA.*

**Background:** High resolution magnetic resonance imaging (MRI) has been successfully utilized in-vivo to discern different internal carotid artery (ICA) plaque components, including the lipid core. High density cholesterol (HDL) is known to have a cardio-protective role believed to be primarily mediated by reverse cholesterol transport. However, HDL is a heterogeneous molecule with 2 major sub-fractions: HDL<sub>2</sub> (large buoyant) and HDL<sub>3</sub> (small dense) and controversy exists regarding the protective role of HDL<sub>2</sub> or HDL<sub>3</sub> in atherosclerosis. We hypothesized that we could utilize high resolution MRI to demonstrate an in-vivo association between HDL sub-fractions and atherosclerotic plaque or its components in the ICA of patients with advanced atherosclerosis.

**Purpose:** To determine the relationship of HDL<sub>2</sub> and HDL<sub>3</sub> with lipid core volume measured in the AP of the ICA imaged using high resolution MRI.

**Methods:** ICA's of 28 patients with known atherosclerosis (mean age 73 ± 4 years, 73% males) were imaged on a 1.5 T CV/i GE MR scanner. Five oblique slices each of the ICA in 3 different weightings (Figure 1): Pre-contrast T1-weighted (TR = 1 R-R, TE = minimum, ETL = 10, FOV = 14 × 14 cm, matrix 256 × 256, 2mm thickness, slice gap = none,

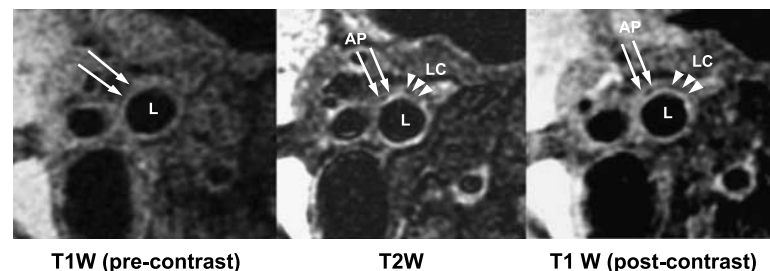


**Figure 1.**

NEX = 1, bandwidth = 62 kHz), T2-weighted (TR = 2 R-R, TE = 69 msec, TI = auto, ETL = 10, FOV = 14 × 14 cm, matrix 256 × 256, 2mm thickness, slice gap = none, NEX = 1, bandwidth = 62 kHz, chemical fat saturation) and T1-weighted (after infusion of 0.1 mmol/kg of intravenous gadodiamide) were obtained and composite vessel wall volume and volume of lipid core was calculated using MASS software (MEDIS, Netherlands). HDL<sub>2</sub> and HDL<sub>3</sub> were calculated from plasma by ultracentrifugation using the vertical auto profile (VAP) technique (Atherotech, Inc, Alabama). Cardiac risk factors, low density cholesterol (LDL), triglycerides (TG) and abdominal girth were recorded.

**Results:** The average scan duration was 50–60 minutes. The mean LC volume and vessel wall volume were  $0.03 \pm 0.03$  and  $0.45 \pm 0.11$  mm<sup>3</sup> respectively. The mean total HDL, HDL<sub>2</sub> and HDL<sub>3</sub> were  $48 \pm 11$ ,  $11 \pm 5$  and  $36 \pm 7$  mg/dl, respectively. On linear regression, there was an inverse correlation between lipid core and HDL<sub>3</sub> ( $r = -0.57$ ,  $p = 0.003$ ) which remained significant after addition of the following confounding variables in a multivariate model: diabetes, gender and abdominal girth ( $R^2 = 70\%$ ,  $R^2$  adjusted = 63 %,  $p < 0.001$ ). For HDL<sub>2</sub>, a trend towards significance ( $r = 0.35$ ,  $p = 0.08$ ) became non-significant after multiple regression analysis ( $R^2 = 60$  %,  $R^2$  adjusted = 21 %,  $p = 0.27$ ). There was no association between vessel wall volume and the HDL sub-fractions.

**Conclusion:** HDL<sub>3</sub> has a significant inverse correlation with the lipid core in atherosclerotic plaque, which can be accurately and non-invasively demonstrated by MR imaging. Relationships for HDL<sub>2</sub> were weaker and non-significant. These results underscore the greater potential role of high resolution MRI in detecting significant in-vivo associations between atherosclerosis and its risk factors in a relatively small population size.

### 308. Assessment of Functional Flow Reserve Using Real-Time Global Coherent Free Precession

Timothy S. E. Albert, MD,<sup>1</sup> Wolfgang G. Rehwald, PhD,<sup>2</sup> Burkhard Sievers, MD,<sup>1</sup> Raymond J. Kim, MD,<sup>1</sup> Robert M. Judd, PhD.<sup>1</sup> <sup>1</sup>Medicine, Duke University Medical Center, Durham, NC, USA, <sup>2</sup>Siemens Medical Solutions, Durham, NC, USA.

**Background:** We have previously described a novel technique for obtaining cine angiography images using global coherent free precession (GCFP) (Rehwald et al., 2004). Utilizing a segmented version of GCFP in an animal model we found GCFP filling distance to be linearly related to blood flow [Klem et al., (submitted)]. Since blood flow is dynamic, varying within the cardiac cycle and under different

physiologic states, we developed a real-time version of GCFP that can rapidly image blood flow during changing physiologic conditions. We hypothesized that this technique could accurately assess functional flow reserve.

**Methods:** Femoral artery blood flow was assessed in 5 healthy volunteers using a clinical 1.5 T Siemens Sonata scanner running a real-time GCFP pulse sequence (2-mm in plane resolution, 20 images/sec). This sequence allows an excitation slice to be moved in 3-dimensions during image acquisition in order to localize vessels of interest and optimize signal. The experimental protocol involved imaging blood flow separately in both legs at baseline and immediately after release of femoral artery occlusions (hyperemia) of 30, 60, and 120 seconds duration.

**Results:** Baseline peak filling distance by GCFP was  $6.5 \pm 1.4$  cm ( $n = 10$ ), falling to 0 cm during occlusion. Peak filling distance after 30, 60, and 120 seconds of occlusion was  $15.0 \pm 2.5$ ,  $18.6 \pm 2.5$ , and  $20.1 \pm 3.3$  cm, respectively. Filling distance increased in a step-wise fashion with increasing

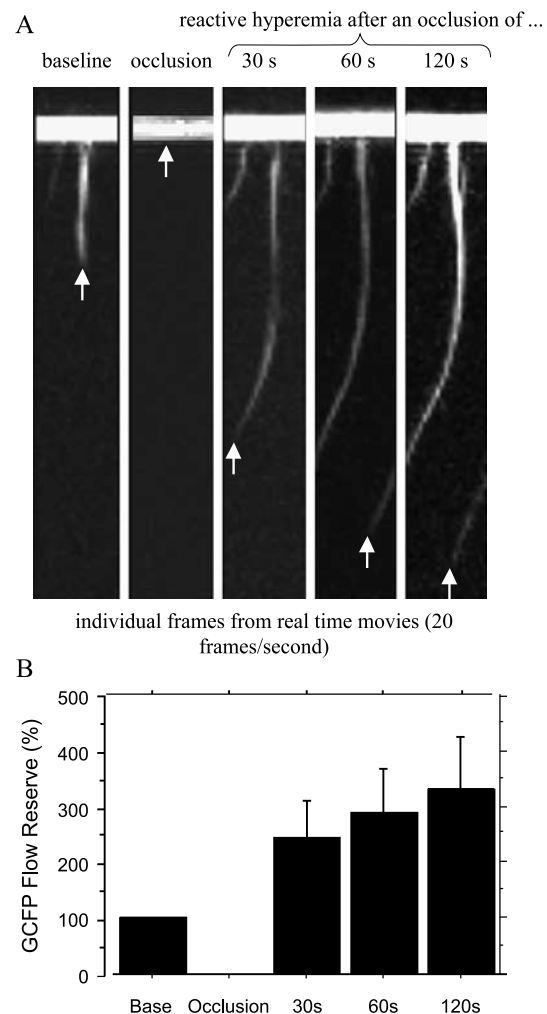


**Figure 1.**

occlusion duration ( $p = 0.001$ ) (see Figure 1A). The reactive hyperemic response after a 120 sec occlusion resulted in increases in GCFP filling distance of  $>300\%$  above baseline (see Figure 1B).

**Conclusion:** Real-time GCFP can be used to non-invasively assess functional flow reserve. These findings suggest that real-time GCFP may be useful as a new form of non-invasive stress testing.

## References

- Rehwald, W. G., et al. (2004). Noninvasive cineangiography by magnetic resonance global coherent free precession. *Nat. Med.* 10:545–549.
- Klem, I., et al. Noninvasive assessment of blood flow based on magnetic resonance global coherent free. submitted.

### 309. Single-Echo Versus Multiple Echo Cardiac T2\* Estimates for Cardiac Iron Estimation in Iron Overload

John C. Wood, MD, PhD,<sup>1</sup> Cathleen Enriquez, BS,<sup>1</sup> Andrew Powell, MD,<sup>2</sup> Niles Ghugre, MS,<sup>1</sup> Marvin Nelson, MD,<sup>3</sup> Jason Polzin, PhD,<sup>4</sup> Thomas D. Coates, MD.<sup>5</sup> <sup>1</sup>Cardiology, Childrens Hospital Los Angeles, Los Angeles, CA, USA, <sup>2</sup>Cardiology, Childrens Hospital Boston, Boston, MA, USA, <sup>3</sup>Radiology, Childrens Hospital Los Angeles, Los Angeles, CA, USA, <sup>4</sup>General Electric Medical Systems, Milwaukee, WI, USA, <sup>5</sup>Hematology, Childrens Hospital Los Angeles, Los Angeles, CA, USA.

**Introduction:** Despite iron chelation therapy, iron cardiomyopathy remains the leading cause of death in thalassemia. Unfortunately, conventional cardiac monitoring fails to reliably identify preclinical disease. Myocardial T2\* measurement has been proposed to identify asymptomatic patients with heavy cardiac iron burdens. Patients with myocardial T2\*  $> 20$  ms have normal cardiac function and rhythm, while those with T2\* less than this value have increasing relative risk of cardiac symptoms, medications, arrhythmias or abnormal function (Anderson et al., 2001; Wood et al., 2004).

To date, we have studied 104 patients with transfusional iron overload using a ECG-gated, multiple breath-hold, single-echo myocardial T2\* technique. This approach is time-consuming and has imperfect image registration between breath-holds. In this abstract, we cross-validate a pre-product echoplanar single-breath-hold T2\* sequence (General Electric) with our previous method. Intermachine differences were also evaluated using a manganese chloride phantom.

**Methods:** Twenty seven patients with thalassemia and sickle cell disease were studied using 1.5 Tesla General Electric MRI

scanners at Children's Hospital Los Angeles (CVi, version 9.1) and Children's Hospital Boston (Twinspeed, version 10.0). Single-echo and echoplanar T2\* measurements were collected from the same single mid-ventricular slice using a 4 element torso coil. Single-echo sequence consisted of a ECG-gated, segmented gradient echo sequence using 4–8 views per trigger and SCOPEG phase encoding. TR was 21 ms, matrix  $128 \times 256$  points, slice thickness 6–8 mm, field of view 36–40 cm, and bandwidth  $\pm 125$  kHz. TE was stepped from 2, 3, 4, 6, 9, 12, 15, and 18 ms on consecutive breath holds. Identical parameters were used for the echoplanar pulse sequence except echo spacings were multiples of one another. Eight echoes were collected (1.7, 3.5, 5.3, 7.1, 8.9, 10.7, 12.5, and 14.3 ms in Los Angeles and 2.2, 4.4, 6.6, 8.8, 11.0, 13.2, 15.4, and 17.6 in Boston).

A T2\* phantom was constructed using plastic bottles of manganese chloride solutions having concentrations of 0.5, 0.75, 1, 1.5, 2, 2.5, 3.5, 5, 8, 12, 16 and 24 mM. Echoplanar T2\* values were measured on both scanners using a single slice collected from the midpoint of the bottles.

All images were fit to monoexponential signal decay with signal offset compensation. Scattergrams, linear correlation, and Bland-Altman statistics were used to compare data from the different sequences and different scanners.

**Results:** For myocardial T2\* values  $< 20$  ms, the echoplanar technique yielded 11% higher values with a standard deviation of 16% compared to the single echo technique. Linear correlation yielded r-value of 0.96 with a slope of 1.13. The two techniques were not statistically correlated in patients having no detectable cardiac iron (T2\*  $> 20$  ms).

For the echoplanar sequence, R2\* was linear with MnCl<sub>2</sub> concentration from R2\* values of 30–900 ms ( $r^2 > .994$ ), nearly 3 times the range observed in human hearts. Bland-Altman agreement between the two scanners was  $1.4 \pm 1.4\%$  for phantom R2\* measurements.

**Discussion:** The echoplanar T2\* implementation exhibits clinically acceptable bias and variability compared with prior single echo techniques. The poor agreement between the two techniques for T2\*  $> 20$  ms indicates that many factors contribute to T2\* measurements in the absence of detectable iron. Fortunately, disparate results in this R2\* range are not clinically relevant. Our results support the findings of Westwood et al. who performed a similar comparison independently on another platform (Westwood et al., 2003). The present echoplanar myocardial T2\* technique offers fast, accurate assessment of cardiac T2\* on General Electric systems 9.1 and higher.

## References

- Anderson, L. J., Holden, S., et al. (2001). *Eur. Heart J.* 22(23):2171–2179.
- Wood, J. C., Tyszka, J. M., et al. (2004). *Blood* 103(5):1934–1936.
- Westwood, M., Anderson, L. J., et al. (2003). *J. Magn. Reson. Imaging.* 18(1):33–39.

### 310. Phase Train Approach for Very High Temporal Resolution Cardiac Imaging

Vinay M. Pai, PhD,<sup>1</sup> Leon Axel, PhD, MD,<sup>1</sup> Peter Kellman, PhD.<sup>2</sup> <sup>1</sup>Radiology, New York University School of Medicine, New York, NY, USA, <sup>2</sup>Laboratory of Cardiac Energetics, National Heart, Lung and Blood Institute, Bethesda, MD, USA.

**Introduction:** We present an approach for obtaining very high temporal resolution (1.5 ms) cardiac images in a breathhold scan. This approach [called phase train imaging (PTI)] is a novel variation on the conventional multiecho SSFP imaging technique. In this approach, each echo in a set of echoes following an RF excitation pulse acquires the same k-space line, and is assigned to a different cardiac phase. When used in conjunction with parallel imaging approaches, this technique permits very high temporal resolution cardiac imaging in a breath-hold duration.

**Purpose:** Very high temporal resolution cardiac MR imaging may prove to be very useful for evaluating mechanical dyssynchrony, a key indicator for chronic heart

failure, especially in early stages of systolic contraction and diastolic expansion. It may also prove useful for studying valvular dynamics.

**Methods:** While multi-echo SSFP techniques (Herzka et al., 2002) have been developed for acquiring high temporal resolution cardiac images, they are naturally restricted to a maximum temporal resolution of 4.5 to 5 ms. This is due to the need to implement techniques to minimize phase discontinuities which can arise due to acquisition of multiple phase-encoding lines per repetition. While single-echo SSFP techniques can provide very high temporal resolution, they are limited in their practical applicability due to the high number of RF pulses, and the reduced persistence of tagged magnetization (when used to acquire tagged cardiac data) and similar magnetization preparation pulses. The phase train approach presented here eliminates the problems associated with both the techniques indicated above. Since all the echoes acquire the same k-space line for different cardiac phases, there is no phase discontinuity associated with this approach; since multiple echoes are acquired, the number of RF pulses is correspondingly lesser than that for single echo sequences, and tags can persist for a much longer duration. Implementation of phase train imaging (PTI) in conjunction with parallel imaging approaches also minimizes the main drawback of this technique: the long breathhold duration otherwise required to obtain reasonable spatial resolution in the phase-encoding direction. Figures 1 and 2 illustrate PTI implementation over a repetition and a cardiac cycle, respectively. As can be seen, the phase train assigns data from each echo of the multi-echo train to a separate cardiac phase, rather than acquiring multiple phase-encode lines (hence the name: phase train imaging). For each phase, only one phase-encode line is acquired per cardiac cycle; this causes the duration of the scan to be longer than a conventional breathhold duration. Utilizing TSENSE (Kellman et al., 2001) (Figure 2) permits reduction of scan time, and enables breathhold scanning. The sequence has been implemented on 1.5T clinical scanners (Siemens Medical Solutions) and high temporal resolution datasets (up to 1.5 ms) have been acquired on human volunteers. For these scans, SENSE rates of 2 to 4, and phase train lengths of

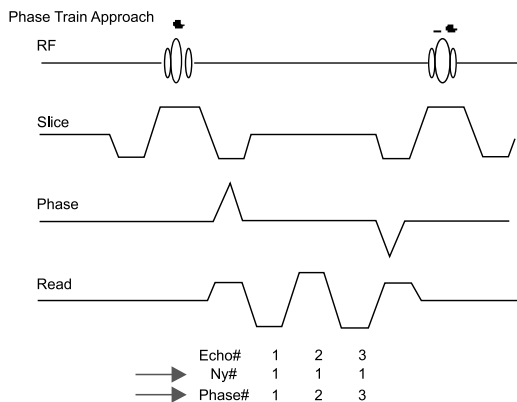


**Figure 1.** Phase train imaging. Each echo acquires a separate cardiac phase for the same phase-encoding. Balanced SSFP conditions are illustrated in this sketch.

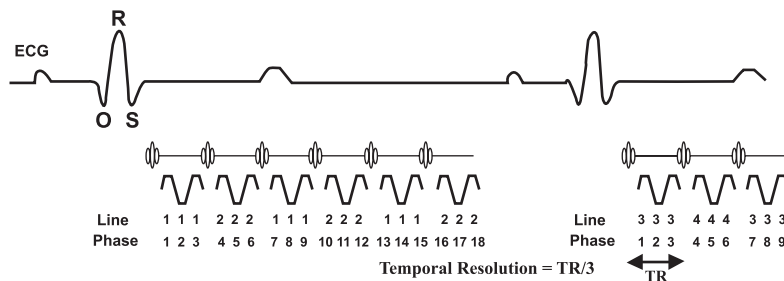


**Figure 2.** Phase train imaging, in combination with TSENSE, over a R-R interval. The schematic illustrates acquisition of k-space lines for SENSE rate of 2, and phase train of 3. TR is the time between successive RF pulses, temporal resolution is TR divided by the length of the phase train, and represents an averaged resolution, as no phases are acquired during the RF pulses.

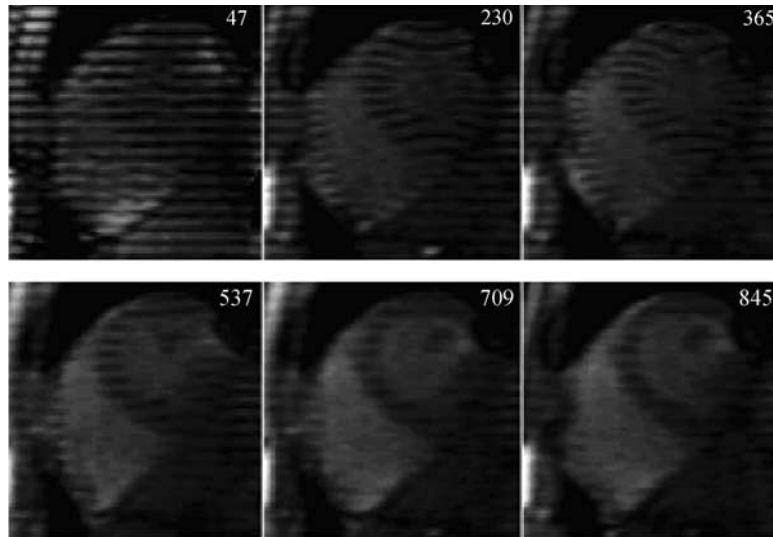


**Figure 3.** Tagged images acquired using phase train imaging (image time stamps shown). SENSE rate:2, phase train 5, flip angle:45, TR: 7.6 ms, breathhold duration 24 s, temporal resolution: 1.5 ms.

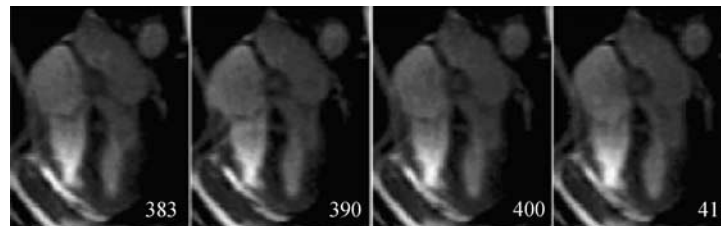


**Figure 4.** Capturing the valvular behavior for tricuspid and mitral valves in early diastole, using phase-train imaging (selected frames shown). SENSE rate: 2, phase train: 3, TR: 5.5 ms, temporal resolution: 1.8 ms, breath-hold duration: 24 s.

3 (TR:6ms) to 5 (TR:7.6ms) were used. Breathhold durations ranged between 12s (SENSE rate: 4) and 24s (SENSE rate: 2).

**Results:** Figure 3 shows representative phases from a cardiac cine data set on a short axis scan (1.5 ms temporal resolution). Figure 4 shows some of the phases from a long-axis scan, capturing the motion of mitral and tricuspid valves in early diastole. While the spatial resolution in the phase-encoding direction is the primary factor influencing breath-hold duration, the temporal and readout resolutions are totally independent of the breathhold duration.

**Conclusions:** Phase train imaging has been developed to obtain very high temporal resolution (up to 1.5 ms) cardiac images in a breath-hold duration. Such high temporal resolution could be useful for applications such as mechanical dyssynchrony and valvular dynamics.

## References

- Herzka, D., et al. (2002). MRM 47(4):655–664.  
Kellman, P., et al. (2001). MRM 46(2):335–343.